Applied Thermal Engineering 248 (2024) 123304

Contents lists available at ScienceDirect

Applied Thermal Engineering

journal homepage: www.elsevier.com/locate/apthermeng

Research Paper

Thermal performance evaluation of hempcrete masonry walls for energy storage in cold weather

Ahmed S. Al-Tamimi [a], Naef A.A. Qasem [b,*], Vivek Bindiganavile [a]

[a] Department of Civil and Environmental Engineering, University of Alberta, Canada
[b] Department of Aerospace Engineering, King Fahd University of Petroleum & Minerals, Dhahran 31261, Saudi Arabia

ARTICLE INFO

Keywords:
Hempcrete
Masonry walls
Thermal performance
Cold weather
Thermal energy

ABSTRACT

During winter, buildings tend to consume a lot of energy for heating due to insufficient insulation of their envelopes. To address this issue, this study explores the use of materials with low thermal conductivity and high specific heat capacity, such as hempcrete, to minimize energy losses through the building envelope. The study suggests optimizing hempcrete components to enhance their thermal properties and evaluates the stored and lost thermal energy to improve the overall thermal performance of building envelopes. Twenty-five hempcretes are experimentally produced and thermally characterized. The thermal assessment also includes some hemp concretes from the literature for comparison purposes. ANSYS Fluent software is used to model the hempcrete walls in a transient state in terms of thermal storage capacity and losses in cold weather (e.g., −20 °C). Results show that stored energy is mainly affected by the product of hempcrete ρ and C_p values, while lost energy depends on thermal conductivity and diffusivity. The highest stored energy over 24 h is observed at 1.91 and 5.54 MJ/m^2 for HC3 (literature) and AAFA-NaOH (present study), respectively, with a difference of 190 %. Further, the lowest values for lost energy are 0.44 and 0.42 MJ/m^2 for HC2 (literature) and S2-CA (present study), respectively. To combine both stored energy and lost energy together, HC2 shows the best performance for the literature walls with lost energy of 0.44 MJ/m^2 and stored energy of 1.82 MJ/m^2; however, the present S2-CA hempcrete has lower lost energy at 0.42 MJ/m^2 and higher stored energy at 3.07 MJ/m^2. Additionally, a present C + Li + 30 % SF hempcrete has a similar lost energy of 0.46 MJ/m^2 but a higher stored energy of 3.36 MJ/m^2. The increasing hemp content has been noticed to increase stored energy by up to 86 % and reduce lost energy by 14.8 %.

1. Introduction

Over the past few decades, building quality has dramatically improved due to rising living standards and advancements in construction materials. Specific regulations were implemented to ensure optimal thermal and acoustic insulation in buildings. A thermally comfortable environment is primarily achieved through heating and cooling systems, which regulate indoor temperature as desired. As a result, varying energy requirements and costs arise due to the influence of external weather conditions and internal climate, which can differ worldwide.

The building envelope encompasses various components, including outer walls, openings such as windows, cladding, external beams and columns, and thermal or cold bridges, which are crucial in regulating heat transfer between the interior and exterior spaces. As a result, they significantly impact the energy consumption of the building. Consequently, it is essential to thoroughly analyze building envelopes to identify areas with inadequate thermal performance. This analysis can inform design and construction decisions to create sustainable buildings and reduce energy consumption. Within the European Union, buildings account for approximately 40 % of the total energy consumption. Precisely, space heating constitutes around 60–80 % of the overall energy consumed by buildings in the European Union [1]. In Canada, space heating makes up about 63 % of total building energy consumption [2], while in the USA, it accounts for approximately 42 % [3]. Enhancing the thermal properties of the building envelope, including improvements in thermal conductivity, density, and specific heat capacity, has the potential to result in significant energy savings. This study focuses on masonry blocks as a prevalent choice for building exteriors worldwide. Concrete masonry units are extensively used in the industry, with an estimated yearly manufacture of around 4.3 billion items in North America (USA and Canada) [4].

Furthermore, governments have established minimum requirements

* Corresponding author.
E-mail address: naefqasem@kfupm.edu.sa (N.A.A. Qasem).

https://doi.org/10.1016/j.applthermaleng.2024.123304
Received 15 January 2024; Received in revised form 27 March 2024; Accepted 28 April 2024
Available online 30 April 2024

Nomenclature

Abbreviations

AAFA	Alkali activated fly ash
AAMK	Alkali activated metakaolin
ASTM	American Society for Testing and Materials
C	Cement
CSA	Canadian Standards Association
FA	Fly ash
GGBS	Ground granulated blast furnace slag
HC	Hempcrete
HIC	High-intensity compaction
HS	Hemp shives
Li	Hydrated lime
LIC	Low-intensity compaction
LWC	Lightweight concrete
MK	Metakaolin
NHL	Natural hydraulic lime
RH	Relative humidity (%)
S	Sand
SF	Silica fume

Symbols

A	Wall area (m^2)
C_p	Specific heat capacity at constant pressure (J/kg K)
C_v	Specific heat capacity at constant volume (J/kg K)
E_{in}	Energy inflow (J)
E_{out}	Energy outflow (J)
E_{st}	Stored Energy (J)
H_{conv}	Convection heat transfer coefficient (W/m^2 K)
k	Thermal conductivity (W/m K)
Nu	Nusselt number
Ql	Lost thermal energy (MJ/m^2)
Qs	Stored thermal energy (MJ/m^2)
q_x	Heat rate (W)
$q_x"$	Heat flux (W/m^2)
T_{amb}	Ambient temperature (°C)

Greek letters

α	Thermal diffusivity (m^2/s)
ρ	Density (kg/m^3)

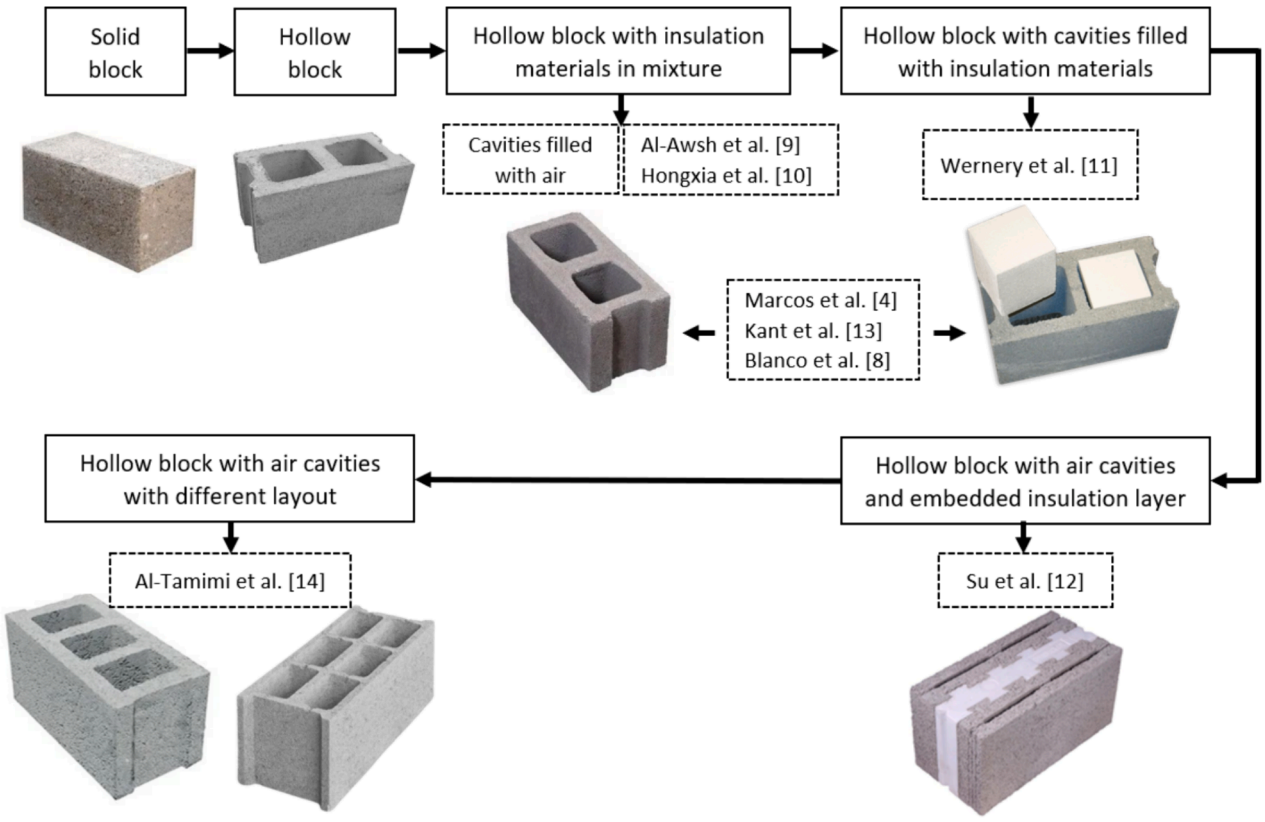

Fig. 1. The literature methods on thermal models with different types of masonry blocks.

for energy efficiency and thermal properties in buildings and construction materials. For example, the legislative body of the European Union [5], CSA [6], and ASTM for concrete masonry units [7] have all implemented regulations pertaining to the thermal insulation of building envelopes. By addressing these factors and adhering to the established standards, significant progress can be made in optimizing buildings' energy efficiency and thermal performance.

Extensive experimental and numerical investigations have been conducted to develop and design masonry blocks that can effectively meet the thermal requirements of building envelopes, ultimately aiming to reduce energy consumption. However, computational fluid dynamics (CFD) is commonly used in many areas of engineering due to the ability to model structures with different materials, shapes, scales, and boundary conditions [8]. Therefore, the thermal behavior of walls is

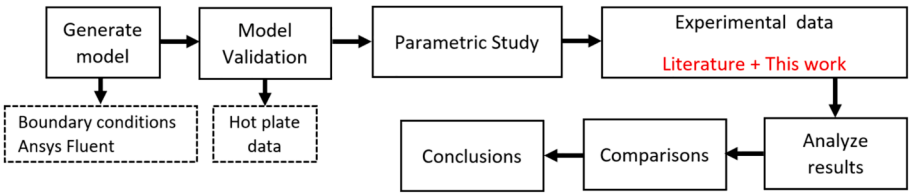

Fig. 2. Methodology of parametric study.

widely modeled, and estimations are demonstrated by real testing for validation [8]. Thermal insulation materials are employed in constructing masonry walls, whether they consist of solid or hollow masonry blocks or are used to fill cavities within blocks. The purpose is to reduce the overall thermal conductivity of the structure.

Many literature studies have conducted thermal models using ANSYS due to the powerful tools for applying boundary conditions for conduction, convection, and radiation for exposed and closed surfaces [910]. Blocks with different types and materials were modeled in ANSYS to evaluate the thermal performance as solid, hollow, and filled cavities with insulation materials, as shown in Fig. 1. Al-Awsh et al. [9] assessed hollow concrete blocks with different insulation materials in the mixture (not filling the cavities), such as low-density polyethylene (LDPE), expanded polystyrene beads (EPS), vermiculite (VL), and volcanic scoria aggregate. The block has the same cavity arrangement layout and dimensions and was tested experimentally using a hot plate device for equivalent thermal conductivity. Thermal Ansys model simulated the test setup of the insulation blocks at steady state, which well matched the experimental outcomes, which proved about 15 % enhancement on the volcanic block's thermal resistance, compared to the control block without insulation materials (same cavities layout and dimensions). The wall surfaces were subjected to boundary conditions involving conduction, convection, and radiation, and cavities were considered filled with air; thus, convection and radiation were included in cavities. Similar boundary conditions were applied by Hongxia et al. [10] to evaluate the sintered coal hollow blocks with ordinary clay blocks in terms of thermal conductivity; thus, the model was conducted at a steady state, which proved an enhancement of coal block with about 65 %.

The effect of filling cavities of hollow blocks with insulation materials was investigated numerically (using BISCO) and experimentally (using a hot-guarded plate) by Wernery et al. [11]. The experimental data showed a significant reduction in thermal conductivity for the hollow blocks filled with aerogel by about 12 % compared to perlite. However, the reduction in thermal conductivity of blocks with filled cavitied with perlite and aerogel could reach 80 and 92 %, compared to unfilled cavities. The two-dimensional model with BISCOO showed an acceptable matching with test results with a difference of less than 12 %. Hollow concrete blocks with an embedded insulation layer of extruded polystyrene were thermally evaluated using the hot box method (steady state) by Su et al. [12]. The test was simulated using ANSYS with the same boundary condition as previous authors, which showed an acceptable matching with an error of less than 6 %.

The hybrid cases of the cavities for the hollow block were targeted experimentally and numerically by Martínez et al. [4], in which cavities were filled with air or insulation materials (cardboard, EPS, and foam). The experimental data was extracted from the hot box test, while the simulation was generated using ANSYS Fluent. The model and experimental results emphasized the importance of convection and radiation, which occurs inside the cavities, on the overall thermal performance of hollow blocks with empty cavities. The results proved the importance of filling the cavities with insulation materials, dramatically improving the blocks' thermal performance, reaching four times. Similar studies include the two scenarios of cavities, such as Kant et al. [13] and Blanco et al. [8], to focus on the improvement and simulation capability of such cases using finite element method (FEM) simulation in ANSYS and COMSOL software to study the thermal behavior of walls made by different type of blocks.

Interestingly, cavities and the layout (arrangements and dimensions) of hollow blocks were explored by Al-Tamimi et al. using ABAQUS [14] to find out how cavities affect heat transfer and optimize cavities layout for better thermal performance. Convection and radiation inside the cavities were applied using ISO standards 6946, and ambient temperatures with exterior solar radiation were utilized as boundary conditions. The resultant cavities layout was patented and optimized for standard block dimensions [15].

The lost energy and required energy were measured using a thermal model in 2-D (using the *Therm* program) and 3-D (using *EnergyPlus*) for an apartment assumed to be located in Lisbon (Portugal) by Real et al. [1]. Four different types of structural lightweight concrete were used in the model to investigate the effect of reducing thermal bridges. However, the thermal properties of the four concretes were measured experimentally in the lab, which are major inputs for the model with the inclusion of boundary conditions. Model outcomes proved a reduction of losing thermal energy between 11–19 %, compared to thermal bridging with normal concrete, while the required energy was reduced by about 20 %. However, this percentage will change with changing climate conditions (location) worldwide. A similar full-scale model was generated for a building using EnergyPlus by Haika et al. [16] to calculate the energy consumption of such a building constructed with hollow concrete blocks, expanded polystyrene (EXP), and hempcrete. The thermal model was supported by full-scale experimental work on the three buildings, which validated the model to a great degree of confidence. Hempcrete showed a promising result with about 82–90 % reduction in the required energy for cooling and heating, compared to hollow concrete blocks.

It is worth mentioning that the previous work by Qasem et al. [17] investigated different concrete types, including hempcrete, based on the literature data. Furthermore, hempcrete, which has superior thermal properties with low thermal conductivity and high heat capacity, was not massively involved in the thermal modeling of building envelopes. Thus, this study experimentally developed some hempcrete and numerically compared their results to those already reported in the literature. This study targets the thermal performance evaluation of hempcrete on storing and losing thermal energy in cold weather countries such as Canada (cold regions in winter such as Alberta) due to the promising thermal properties and potential noticed from literature about hempcrete with low thermal conductivity and high heat capacity. The external temperature of −20 °C is an example to facilitate the comparison among different hempcretes. The methodology employed in this study introduces novel approaches. Firstly, it involves investigating the thermal properties on a small scale, enabling the optimization of hemp components to enhance their properties before scaling up. Secondly, it entails modeling the thermal performance (heat storage and loss) on a large scale, representing building envelopes. Moreover, the reported hempcrete walls in the literature are considered for a comprehensive evaluation and comparison with the newly produced ones. The ANSYS Fluent-based model evaluates energy loss and storage after being validated against hot plate experimental data. The study explores the effect of hempcrete's thermal diffusivity (i.e., ρ, C_p, k) on transient heat transfer to suggest the best hempcrete for cold weather conditions.

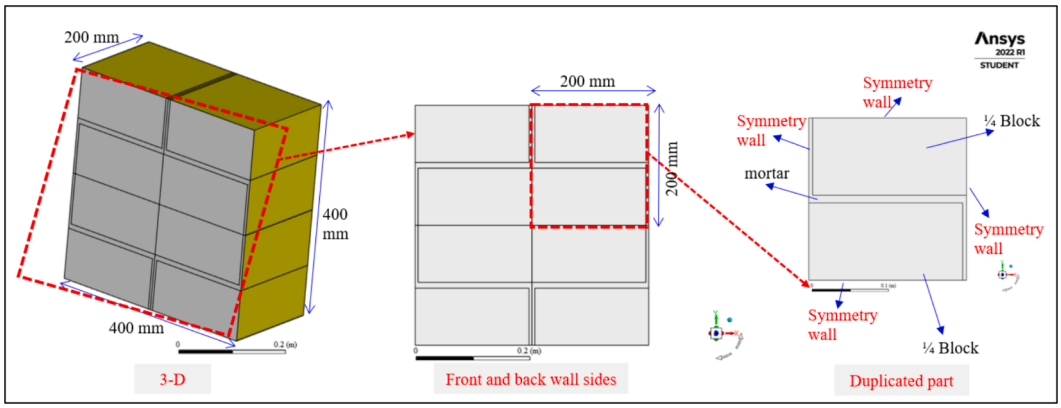

Fig. 3. The model incorporated a masonry wall and its symmetric counterpart.

2. Research methodology

Fig. 2 shows the methodology followed to achieve the objectives of this study. First, the authors explored thermal models in literature for building envelope assessment, the available thermal simulation software, boundary conditions, and preferred results. Then, the transient thermal model was created and verified with experimental data from the literature for the hot plate test. Two groups of data were collected to achieve the goals of this study, as illustrated in Section 2.4. Finally, the model results were summarized, analyzed, and compared to attain inferences about stored and lost thermal energy in/from the building envelope and a richer understanding of the influencer factors.

2.1. Mathematical model

As shown in Fig. 3, a 400 x 400 mm wall was duplicated of part 200 x 200 mm using ANSYS Fluent to assess the thermal efficiency of hempcrete as a solid brick wall. The model followed the principles of the energy conservation equation and accounted for transient heat transfer. Thus, hempcrete walls could be evaluated for the thermal energy stored and lost over the day (24 h). The heat transfer by convection and radiation was considered on both wall surfaces. The mortar is bonded to the block units, forming a cohesive structure with distinct thermal properties. However, the connection zones were considered perfect bonds with no gaps or friction (similar consideration by [9]).

2.1.1. Governing equations

Eq. (1) formulates that the energy equation without radiation in one direction governs the transient heat flow [18].

$$E_{stored} = E_{in} - E_{out} \tag{1}$$

In the given context, E_{stored} represents the energy stored within the fence, E_{in} denotes the energy transferred from the warm room to the fence, and E_{out} signifies the energy escaping from the fence to the chilly outdoor climate.

The stored thermal energy within the wall system can be quantified as follows:

$$E_{stored} = \int \left(C_p \rho \frac{\partial T}{\partial t} dxdydz \right) dt \tag{2}$$

The rate of thermal conduction (q_x in W or J/s) can be estimated from Fourier's law:

$$q_x = -kdA\,\nabla T) \tag{3}$$

Now, the transient heat transfer equation in, incorporating stored energy and conduction through the wall:

$$C_p \rho \frac{\partial T}{\partial t} = \nabla.(k \nabla T) \tag{4}$$

Eq. (4) could be expressed in terms of thermal diffusivity, as in Eq. (5):

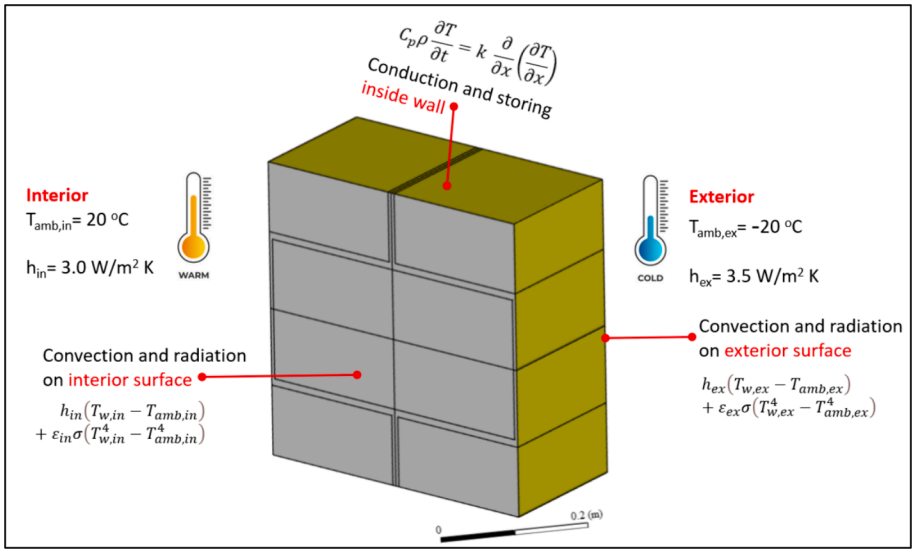

Fig. 4. The heat transfer simulation utilized in this study employed specific boundary conditions.

Table 1
Mesh independence study.

Time (s)	Cell size (m)						
	0.013	0.01	0.008	0.006	0.005	0.004	0.0034
External wall temperature (K)							
0	293.15	293.15	293.15	293.15	293.15	293.15	293.15
10,000	264.5	264.48	264.47	264.47	264.47	264.48	264.5
20,000	261.61	261.6	261.59	261.6	261.6	261.62	261.64
30,000	260.27	260.26	260.26	260.27	260.27	260.29	260.31
40,000	259.38	259.37	259.37	259.38	259.38	259.4	259.43
50,000	258.76	258.75	258.75	258.76	258.77	258.79	258.81
60,000	258.31	258.31	258.31	258.32	258.33	258.35	258.37
70,000	257.95	257.95	257.95	257.95	257.96	257.98	258.01
80,000	257.65	257.65	257.65	257.66	257.67	257.69	257.72
%Difference at 80000 s	0.027 %	0.027 %	0.027 %	0.023 %	0.019 %	0.012 %	0

$$\frac{\partial T}{\partial t} = \alpha \nabla^2 T \tag{5}$$

2.1.2. Boundary conditions

Thermal transfer between the fence (wall) surfaces and their respective ambient environments occurs through separate convection and radiation processes on each surface, as expressed in Eqs. (6) and (7) [9].

$$k_w \nabla T_{w,ex} = h_{ex}\left(T_{w,ex} - T_{amb,ex}\right) + \varepsilon_{ex}\sigma\left(T_{w,ex}^4 - T_{amb,ex}^4\right) \tag{6}$$

In the given context, the variables are defined as follows:

k_w represents the thermal conductivity coefficient of the wall materials (W/m K).

h_{ex} denotes the convection heat transfer coefficient on the exterior surface (W/m^2 K).

$T_{w,ex}$ corresponds to the temperature of the outer wall facade (K).

$T_{amb,ex}$ represents the surrounding temperature outside the building (K).

ε_{ex} signifies the emissivity factor of the external wall surface.

σ represents the Stefan–Boltzmann constant (5.6703 $\times$ 10^{-8} W/m^2 K^4).

Likewise, regarding the interior wall,

$$k_w \nabla T_{w,in} = h_{in}\left(T_{w,in} - T_{amb,in}\right) + \varepsilon_{in}\sigma\left(T_{w,in}^4 - T_{amb,in}^4\right) \tag{7}$$

It should be noted that the radiation heat transfer from the internal wall to the room walls and from the external wall to the surroundings is assumed to be from a wall to a closed enclosure with a view factor of 1. The room walls' temperature is assumed to be room temperature, and the external enclosure is assumed to be ambient temperature.

The convection heat transfer coefficients at the vertical walls were estimated using Eq. (8), and more details about calculations could be found [18]:

$$h = \frac{Nu^* k_{air}}{L} \tag{8}$$

where k_{air} represents air thermal conductivity, L corresponds to the wall's vertical length, and Nu is the Nusselt number.

By employing the equations above, the convective coefficients for the surfaces of the inner and outer walls were determined to be 3 and 3.5 W/m^2 K, respectively. Fig. 4 illustrates the comprehensive boundary conditions applied to the wall. It's important to highlight that the paper overlooks wind speed and assumes a consistent temperature inside and outside to simplify the compression of various walls. The paper does not concentrate on estimating energy consumption under variable and precise conditions.

2.2. Mesh independence

Mesh was verified in this study to ensure the quality of model results. Thus, nine trials with various numbers of cells (0.40, 1.0, 7.0, 16.0, 31.0, 73.0, 128, 250, and 411 k) were examined, representing cell sizes 35 – 3.4 mm, as illustrated in Table 1. Mesh verification was assessed regarding the external wall temperature (T_{ex}) with elapsed time and meshing cell size (0.013, 0.01, 0.008, 0.006, 0.005, 0.004, and 0.0034 m), as presented in Table 1. The external wall temperature shows almost the same results for all the studied mesh schemes. However, to ensure mesh independence for all modeled cases, the smallest mesh cell size of 0.0034 mm (with a total of mesh cells 411,000) is implemented in this study.

2.3. Model validation

For model validation, an experimental study was selected from the

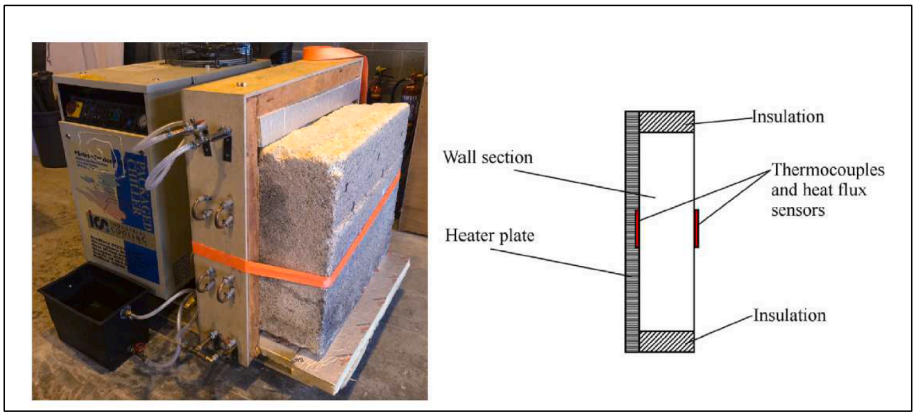

Fig. 5. The hot plate device configured with a sample of lime hemp concrete for experimental testing [19].

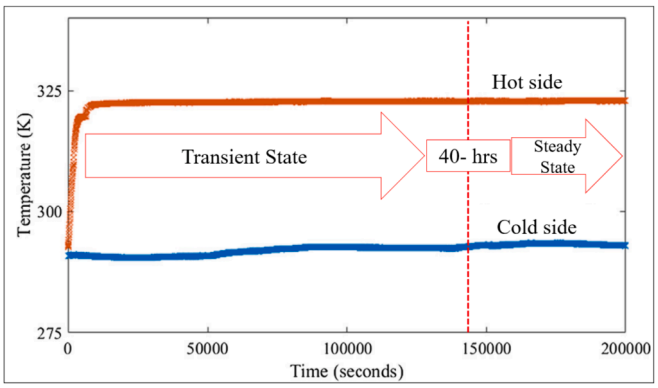

Fig. 6. Experimental temperature data for hot and cold surface of hempcrete sample [19].

Table 2
The model's input parameters include various factors and variables that are utilized to describe and simulate the system under study.

Geometric	Materials Properties	Conditions
Wall width = 0.30 *m*	k = 0.129 W/m K	T_{hot} = 51 °C
Wall area = 0.90x0.90 *m*	C_p = 1627 J/kg K	T_{cold} = 20 °C
	ρ = 508 kg/m^3	Transient time = 300,000 s

literature about testing hempcrete walls for thermal conductivity using the hot plate method [19]. As shown in Fig. 5, a hempcrete wall of about 1 m^2 and a width of 0.30 m was installed on the test setup, where the hot plate was in contact with the wall surface and the other wall surface was exposed to ambient conditions [19]. Additionally, temperature and thermal flow sensors were installed on both wall surfaces to measure and track the temperature and heat flux at the surface.

Testing started with setting the heater temperature at 60 °C, heating the wall surface, causing a temperature gradient, and flowing heat toward the cold side of the wall (ambient). The temperature and heat flux were monitored on both wall surfaces to ensure reaching a steady state, achieved after about 40 h [19], as shown in Fig. 6 for temperature monitoring.

The experimental data in Table 2 was used for model verifications, which attained a reasonable agreement with the experimental data (about < 7 %), as shown in Fig. 7. The geometric, material properties, and wall conditions listed in Table 2 were sourced from a literature-based experimental study [19] to validate the model.

Fig. 7 illustrates that the heat flux steadily increases during the transient state (Time = 0 to 40 h) from zero to about 10 W/m^2. This is attributed to the dominance of thermal diffusivity (represented by the values of k and C_p) in governing heat transfer at this stage. During this period, the material absorbs heat until it reaches full charge, after which heat conduction stabilizes and undergoes minimal changes, as there is no longer stored heat within the material, and the difference between 40 hr and ending the test in less than 16 %. Fortunately, the modeling results of heat flux demonstrate the reasonable matching (not exceeding 7 % after 200000 s) between the experimental data exported from the literature [19] and the simulation results generated in this study, as presented in Fig. 7.

The model results disparity becomes pronounced during the early phase of experiments but stabilizes beyond 200,000 s with a variance of less than 6 %. This trend is attributed to heat dissipation during the initial stages of thermal transfer, where the heat generated gradually escalates until reaching a stable state. Thus, the model's early-stage heat flux showed a consistent and gradual elevation of heat flow until reaching steady.

2.4. Materials and data

This study used two categories of materials, including literature concretes and hemp concretes, which were produced and tested in the lab for their thermal properties. The model involved constructing a wall measuring 1 m x 1 m by assembling blocks with dimensions of 40 cm x 40 cm x 20 cm. The wall was built using two types of mortars, cement mortar, and lime mortar, depending on the concrete binder used.

2.4.1. Hempcrete I: From literature

Extensive data from various literature sources were gathered, encompassing different concrete formulations. These data included information on thermal properties such as density, thermal conductivity (k), specific heat capacity (C_p), and thermal diffusivity (α), resulting in a dataset of approximately 400 concrete mixtures. The collected data underwent four sorting procedures: (1) Low to high order for thermal conductivity, (2) diffusivity, and (3) density; (4) High to low order for

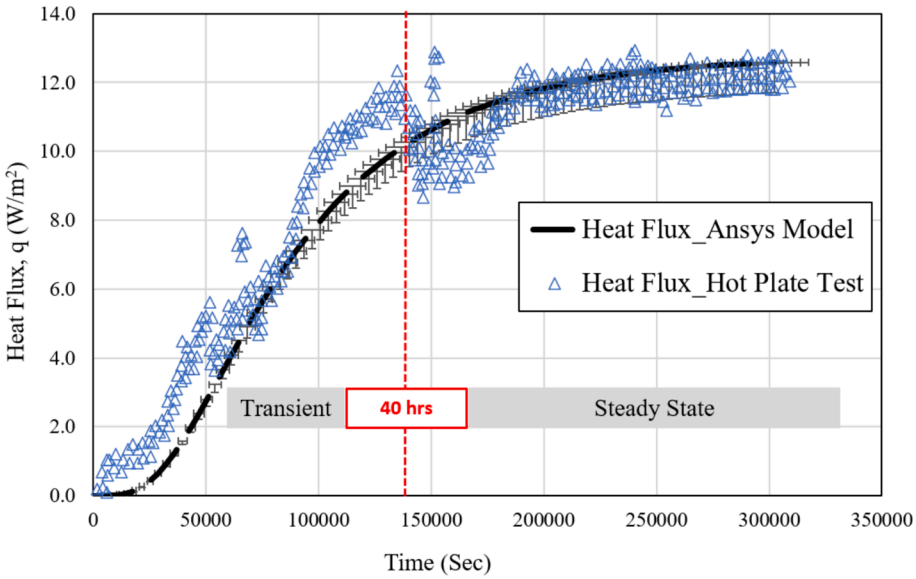

Fig. 7. The temporal heat flux values for the wall cold surface obtained from the model were compared with the corresponding experimental data to validate the model.

Table 3
Thermal properties of various concrete types obtained from literature .

Mix No.	Mixture	binder/ hemp	density	*k-value*	C_p-*value*	*α-value*	Ref.
			kg/m^3	W/m K	J/kg K	m^2/s	
HC11	C + HS (S1 < 10 mm)- LIC	2.0	351	0.105	650	0.46 × 10^{-6}	[20]
HC9	C + HS (S2 < S1)- LIC	2.0	340	0.103	750	0.40 × 10^{-6}	
HC13	C + HS (S1 < 10 mm)- HIC	2.0	415	0.110	690	0.38 × 10^{-6}	
HC12	C + HS (S2 < S1)- HIC	2.0	410	0.115	760	0.37 × 10^{-6}	
HC6	Li + NHL5 + FA + HS- (RH = 15 %)	1.10	1001	0.094	333	0.28 × 10^{-6}	[21]
HC8	Li + NHL5 + FA + HS- (RH = 65 %)	1.10	1111	0.100	300	0.30 × 10^{-6}	
HC10	Li + NHL5 + FA + HS- (RH = 15 %)	1.80	995	0.105	385	0.27 × 10^{-6}	
HC7	Hempcrete	NA	413	0.100	1000	0.24 × 10^{-6}	[22]
HC4	Hempcrete for External Wall- Trade	NA	275	0.060	1500	0.15 × 10^{-6}	[23]
HC3	Hempcrete for floor- Trade		330	0.070	1550	0.14 × 10^{-6}	
HC2	TRADICAL hempcrete- Trade		275	0.060	1800	0.12 × 10^{-6}	

Sources

(a) (b)

Fig. 8. (a) Hemp hurds aggregate; (b) Hempcrete samples disc for thermal properties measurements.

Table 4
Mix proportions of hempcrete with various binders, hemp sizes, and the same binder-to-hemp ratio.

Mix composition (% by wt.)	water/ binder	water/binder (Including abs.)
100 % C + 40 % HS	0.35	1.15
70 % C + 30 % SF + 40 % HS		
70 % C + 30 % FA + 40 % HS		
70 % C + 30 % MK + 40 % HS		
70 % C + 30 % GGBS + 40 % HS		
70 % C + 30 % Li + 40 % HS		
100 % Li + 40 % HS	0.90	1.70
70 % Li + 30 % SF + 40 % HS		
70 % Li + 30 % FA + 40 % HS		
70 % Li + 30 % MK + 40 % HS		
70 % Li + 30 % GGBS + 40 % HS		
70 % Li + 30 % C + 40 % HS		
50 % C + 50 % Li + 40 % HS	0.625	1.42
35 % C + 35 % Li + 30 % SF + 40 % HS		
35 % C + 35 % Li + 30 % FA + 40 % HS		
35 % C + 35 % Li + 30 % MK + 40 % HS		
35 % C + 35 % Li + 30 % GGBS + 40 % HS		
AAFA- NaOH + 40 % HS	0.67	–
AAMK- NaOH + 40 % HS	1.26	
AAFA- (NaOH + Na_2SiO_3) + 40 % HS	0.80	
AAMK-(NaOH + Na_2SiO_3) + 40 % HS	1.38	
(AAFA + AAMK)- (NaOH + Na_2SiO_3) + 40 % HS	1.09	
50 % C + 50 % Li + 40 % HS (**S4-FR**)	0.625	1.42
50 % C + 50 % Li + 40 % HS (**S1-CA**)		1.42
50 % C + 50 % Li + 40 % HS (**S2-CA**)		1.71
50 % C + 50 % Li + 40 % HS (**S3-CA**)		1.82

specific heat capacity. This ensured that the modeling process accounted for concretes with the lowest thermal conductivity, diffusivity, and density values and the highest heat capacity value. Ten concrete mixtures from each group that had been sorted were chosen for additional modeling purposes. Hempcretes were assembled, as summarized in Table 3.

2.4.2. *Hempcrete II: Present experimental data*

An experimental program was conducted to study the thermal properties of hempcrete in the first phase of this study. Four groups of binders were investigated for strength and thermal properties, including cement-based, lime-based, cement-lime-based, and alkali-activated. However, the binder-to-hemp ratio was fixed (2.50), and the hemp size was the same (S4-FR) supplied by LCDA in France. It also met all technical standards of French hemp building professional rules, as shown in Fig. 8. The mix design of hempcrete is according to the absolute volume method (ACI 211) [24]. The composition of each mixture is detailed in Table 4, showing four groups of binders and four hemp sizes for the same binder-to-hemp ratio to explore the effect of binder and hemp size on thermal properties and thermal performance using the Fluent model.

Hemp hurds offer a thermal insulation advantage over hempcrete; however, they also significantly affect the binder matrix, reducing bonding, strength, and compatibility between them. In summary, the critical effects can be sugar [2526], pectin [2728], water absorption [2930], and the flaky shape of hemp particles [31]. Therefore, different types of binders and hemp sizes were investigated experimentally and assessed numerically using the Fluent model.

The components were mixed (binder + hemp + water) using a rotary pan mixer. The homogeneous mixture was then poured into a disc with a

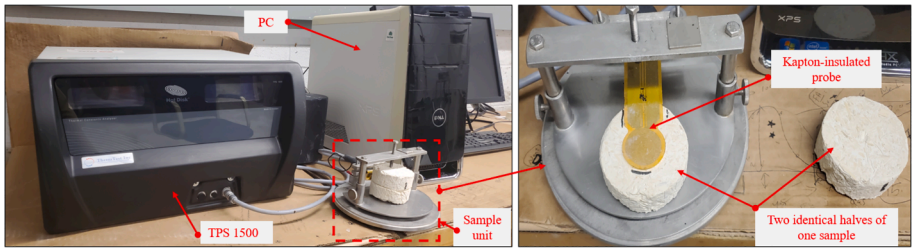

Fig. 9. TPS 1500- Thermal Constant Analyzer with a sample unit.

diameter of 75 mm and a thickness of 30 mm. The next samples were cured for 28 days in a humidity room. After that, samples were dried in the oven for 24 h at 60 °C. Finally, one surface was ground to flatten it (Fig. 8) and be ready for the thermal test.

The thermal diffusivity and conductivity were assessed using the transient plane source (TPS) measurement technique called Hot Disk Method (HDM) [32]. TPS 1500 has three probes: Kapton, Mica, and Teflon sensors. In this study, Hot Disk TPS 1500 (thermal constants analyzer) was used to measure the thermal constants of the prepared samples of hemp concrete with an accuracy better than 5 % according to ISO 22007–2 [32]. As shown in Fig. 9, the setup mainly comprises a TPS-1500, PC, and Kapton-insulated probe with a 14.60 mm radius embedded horizontally between two halves of the tested specimen. The hot disk acts as a heat source and resistance thermometer to raise the sample temperature and record time-dependent temperature increase [32].

The principle of the Hot Disk Method is to produce a heat pulse for a defined period (by electrical current) in the form of a stepwise function through a hot disk sensor to generate a dynamic temperature field within the specimen's two halves [32]. The increase in the average temperature of the hot disk probe is measured as a function of time by monitoring the electrical resistance of the probe (sensor or adaptor) [3233]. Eqs give the solution of the thermal conductivity Eqs. (9) and (10):

$$\Delta T_s(\tau) = \frac{P_o}{\pi^{1.5} r k} D(\tau) \tag{9}$$

$$\tau = \sqrt{\frac{\alpha(t - t_c)}{r^2}} \tag{10}$$

where $\Delta T_s(\tau)$ is the temperature increase of the sample surface, P_o is the output power from the probe, r is the radius of the probe, k is the thermal conductivity of sample, $D(\tau)$ is a dimensionless specific time function [32], α is thermal diffusivity of sample, t is the total measurement time, t_c is time correction less than 0.5 % of the total time because the development of full output power does not coincide precisely with $t = 0$.

To solve Eq. (9), an iteration procedure with diffusivity (α); time correction (t_c) is established, and a linear relationship between $\Delta T_s(t)$ and $D(\tau)$ is created. The values of α and t_c were obtained from the last step of iteration. Finally, thermal conductivity is the slope of the generated line.

Finally, the volumetric heat capacity (C_v) could be obtained by dividing thermal conductivity by thermal diffusivity.

$$C_v = \frac{k}{\alpha} \tag{11}$$

If the bulk density of samples is available, the specific heat capacity (C_p) could be calculated.

$$C_p = C_v/\rho \tag{12}$$

The thermal properties (k, α, C_p) were measured for three samples from each mixture and three readings for each sample. Thus, the measured properties are the average of nine readings (3 readings/sample) with a

Table 5
Thermal properties of experimental hempcrete in this study.

Mix ID	ρ	k	C_p	α
	kg/m^3	W/m K	J/kg K	m^2/s
100 % C + 40 % HS	549.08	0.11	1578.88	0.13 × 10^{-6}
70 % C + 30 % SF + 40 % HS	527.94	0.11	1844.03	0.11 × 10^{-6}
70 % C + 30 % FA + 40 % HS	507.35	0.09	1719.17	0.10 × 10^{-6}
70 % C + 30 % MK + 40 % HS	511.34	0.09	1654.11	0.11 × 10^{-6}
70 % C + 30 % GGBS + 40 % HS	529.24	0.10	1559.81	0.12 × 10^{-6}
70 % C + 30 % Li + 40 % HS	534.44	0.11	2061.86	0.10 × 10^{-6}
100 % Li + 40 % HS	476.27	0.10	1863.79	0.11 × 10^{-6}
70 % Li + 30 % SF + 40 % HS	445.61	0.09	1456.63	0.14 × 10^{-6}
70 % Li + 30 % FA + 40 % HS	446.17	0.10	1571.34	0.15 × 10^{-6}
70 % Li + 30 % MK + 40 % HS	459.88	0.09	1782.59	0.11 × 10^{-6}
70 % Li + 30 % GGBS + 40 % HS	507.22	0.15	1624.93	0.18 × 10^{-6}
70 % Li + 30 % C + 40 % HS	542.83	0.18	2024.56	0.16 × 10^{-6}
50 % C + 50 % Li + 40 % HS	527.07	0.13	1524.87	0.16 × 10^{-6}
35 % C + 35 % Li + 30 % SF + 40 % HS	533.37	0.10	1862.62	0.11 × 10^{-6}
35 % C + 35 % Li + 30 % FA + 40 % HS	546.13	0.16	1798.82	0.16 × 10^{-6}
35 % C + 35 % Li + 30 % MK + 40 % HS	617.64	0.19	1796.17	0.17 × 10^{-6}
35 % C + 35 % Li + 30 % GGBS + 40 % HS	553.21	0.11	1485.41	0.14 × 10^{-6}
AAFA- NaOH + 40 % HS	836.82	0.22	1981.22	0.13 × 10^{-6}
AAMK- NaOH + 40 % HS	718.66	0.15	1512.48	0.14 × 10^{-6}
AAFA- (NaOH + Na_2SiO_3) + 40 % HS	724.25	0.21	1990.91	0.15 × 10^{-6}
AAMK-(NaOH + Na_2SiO_3) + 40 % HS	724.70	0.16	1651.03	0.13 × 10^{-6}
(AAFA + AAMK)- (NaOH + Na_2SiO_3) + 40 % HS	773.35	0.21	1910.58	0.14 × 10^{-6}
50 % C + 50 % Li + 40 % HS (S4-FR)	548.45	0.13	1571.42	0.15 × 10^{-6}
50 % C + 50 % Li + 40 % HS (S1-CA)	505.34	0.11	1595.67	0.14 × 10^{-6}
50 % C + 50 % Li + 40 % HS (S2-CA)	434.47	0.07	1557.55	0.11 × 10^{-6}
50 % C + 50 % Li + 40 % HS (S3-CA)	566.57	0.10	1565.99	0.11 × 10^{-6}

Table 6
Thermal properties of mortars used in this study.

Depth (mm)	Mortar Type	Density (kg/m^3)	*k*-value (W/m K)	C_p-value (J/kg K)	*α*-value (m^2/s)	*ε*-factor	Ref.
10	Cement	2143	0.42	570	0.34 × 10^{-6}	0.90	[4]
	Lime	1251	0.25	960		0.90	

coefficient of variance (COV) less than 10 %. The experimental results of hempcrete mixtures were summarized, as shown in Table 5.

As indicated in Table 6, cement and lime mortars were employed to connect the blocks, which were used with the same binder of the block. However, the emissivity coefficient is assumed to be the same for all walls for model simplicity and lacks values for all concretes. According to the literature, the emissivity factors for brick surfaces typically fall within the range of 0.85 to 0.95 [4]. For this study, an average value of 0.90 was adopted to represent the emissivity coefficient throughout the investigation.

3. Results and discussion

For the experimental data, 26 mixtures were prepared and tested for thermal properties, including thermal conductivity, diffusivity, and heat capacity, before evaluating the thermal performance of such concretes

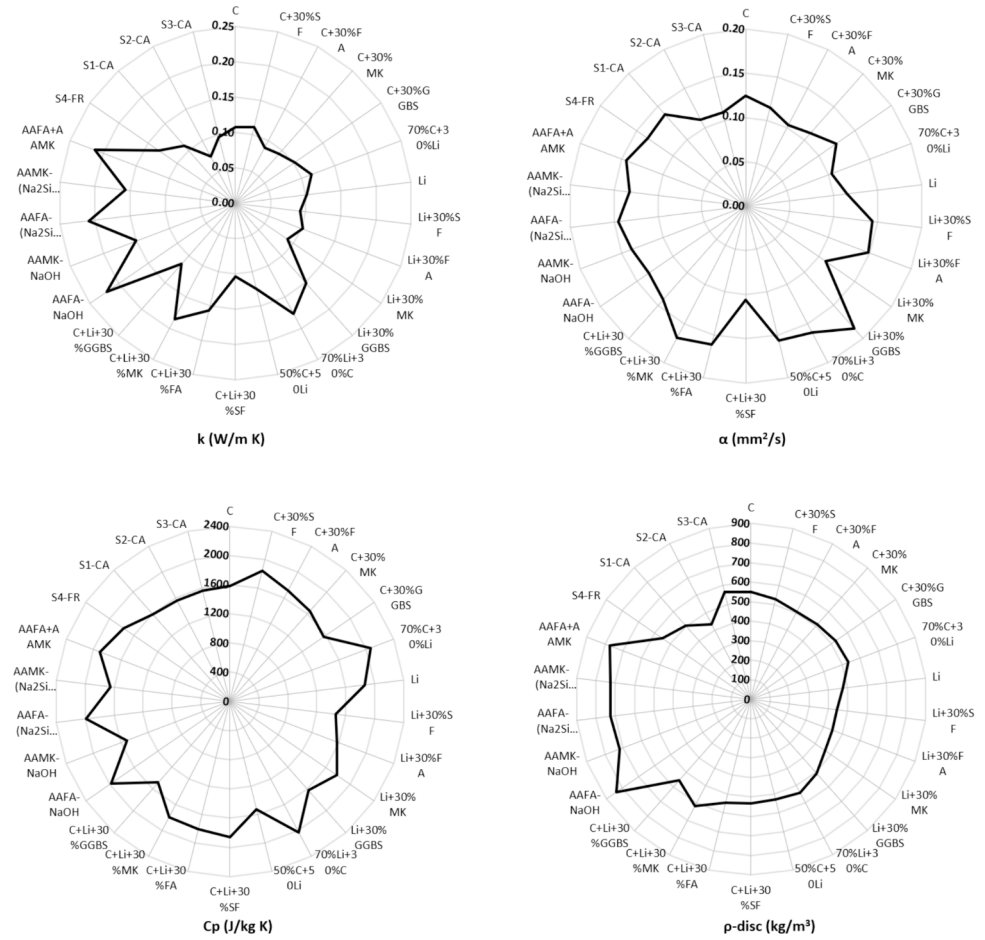

Fig. 10. Thermal properties of hempcrete with various binders, hemp sizes, and the same binder-to-hemp ratio (*k*: thermal conductivity, *α*: thermal diffusivity, C_p: specific heat capacity, *ρ*: bulk density).

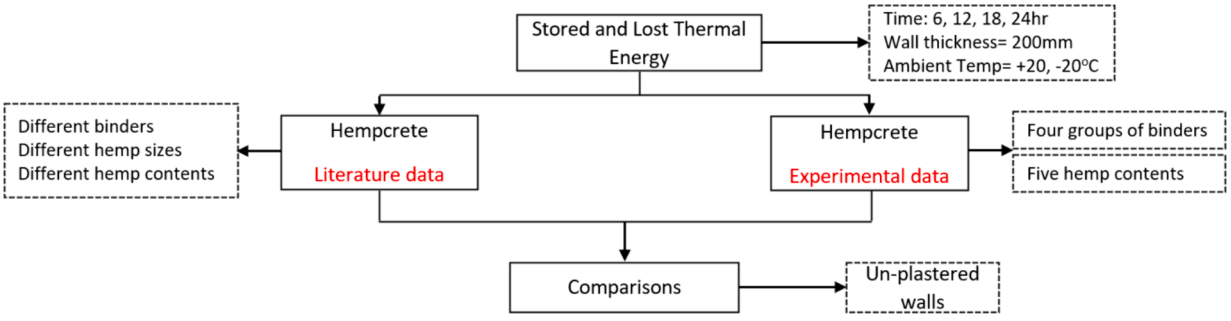

Fig. 11. Milestones of parametric study.

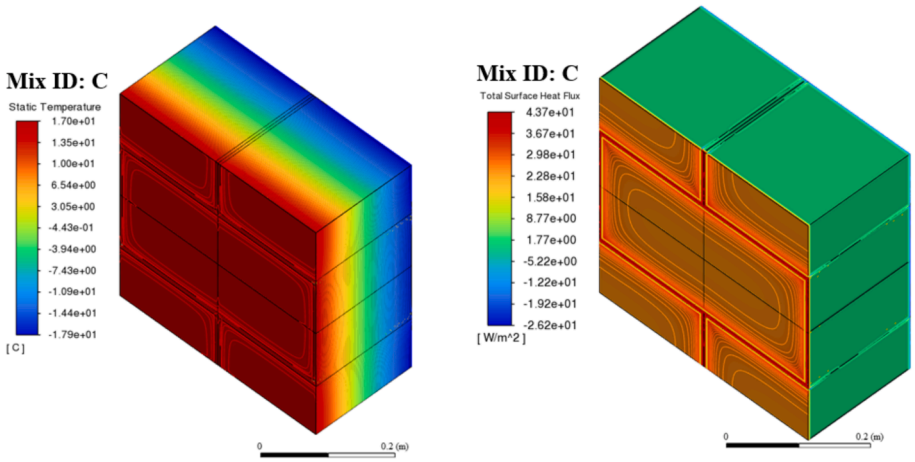

(a)

Fig. 12. Typical three-dimensional contours depicting temperature and thermal flow distributions.

for building envelopes. Fig. 10 shows the difference between all mixtures of hempcrete with four groups of binders and four hemp sizes for the fixed binder-to-hemp ratio to assess the impact on thermal properties. The conductivity of cement-based binders is mostly the lowest, and geopolymers are almost the highest. The lowest water-to-binder ratio for cement binders formed a relatively less workable mixture, leading to a more porous structure. In contrast, alkali-activated binders were less affected by hemp due to the higher production of CSH and NASH. The amount of lime and alumina differed in all binder compositions to optimize the sufficient content to overcome the negative effect of hemp pectin and sugar without chemical treatment. The individual values of thermal diffusivity are varied for each binder composition, reflecting the rate of heat diffusion throughout the samples, which is affected by incorporated factors such as porosity structure, moisture content, amorphous and crystalline structure, and hemp particle arrangement in the heat flow direction. Future studies could be conducted into the microstructure of hempcrete and thermal data analysis for sufficient samples because the standard deviation for thermal diffusivity is mostly higher than the conductivity. The specific heat capacity values are in the range of 1600 – 2000 J/kg K for the dry condition of hempcrete samples with different hemp sizes and binder types, showing a difference of about 20 % ascribed to porosity and binder hardened products.

The first step in this parametric study is generating the thermal model considering the proper boundary conditions and material properties. Then, the model validation process with experimental data from the literature was conducted using the hot plate method. Finally, the model was run with two groups of thermal data for hempcrete, including literature experimental data and this study's experimental data, as illustrated in Fig. 11. The walls were not plastered in this case because the target is to evaluate the difference between the hempcrete of the literature and this study in terms of storing and losing heat capabilities. The experimental results and simulation are complementary because the materials' thermal properties obtained from the test were utilized in the thermal model for a wall to assess the heat efficiency from the perspective of storing and losing thermal energy.

The objective of this study, as depicted in Fig. 11, is to evaluate the thermal performance of various wall systems in terms of thermal energy storage and loss. Therefore, it is crucial to assess the influence of time, specifically at intervals of 6, 12, 18, and 24 h. To simplify the model, the inner and outer sink/ambient temperatures were presumed to remain constant. Additionally, the wall thickness was kept constant at 200 mm, and any variation in thickness was not considered within the scope of

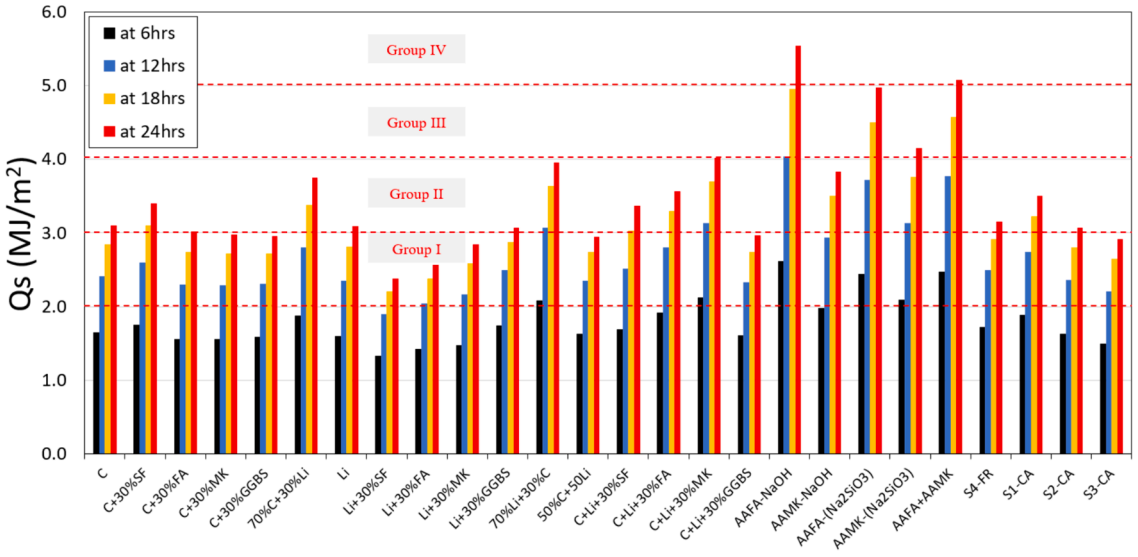

Fig. 13. Stored heat energy is stored in hemp concrete walls produced in this study.

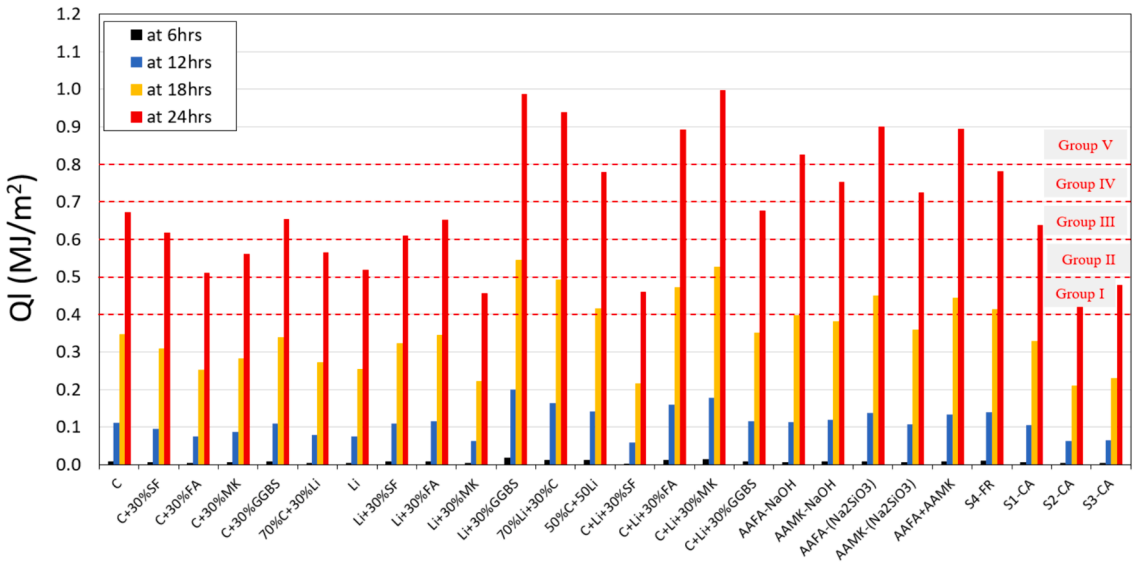

Fig. 14. Lost heat energy in hemp concrete produced in this study.

this study.

The model provided results for various parameters, including inner surface temperature, outer surface temperature, average wall temperature, and thermal flow. These results allowed for the estimation of the total storage and energy losses. Fig. 12 presents typical three-dimensional visualizations of masonry block walls. The figure demonstrates an amplified temperature gradient and heat flux at the connection zones (mortar) compared to the blocks. This is attributed to thermal bridging caused by the relatively higher thermal properties of the mortar.

3.1. Stored and lost heat energy for hempcrete II

The experimental data for the thermal properties of hempcrete, including conductivity (0.07 – 0.22 W/m K), diffusivity (0.10 – 0.17 × 10^{-6} m^2/s), and C_p (1460 – 2060 J/kg K) are shown in Fig. 10. The highest density is for wall AAFA-NaOH (837 kg/m^3), and heat capacity for 70 %C + 30 %Li (2060 J/kg K), while the lowest thermal conductivity is for S2-CA (0.070 W/m K), and thermal diffusivity for 70 %C + 30 %Li and 70 %C + 30 %FA (0.10 × 10^{-6} m^2/s). For the literature hempcrete, the range of measured properties is as follows: thermal conductivity (0.06 – 0.115 W/m K), diffusivity (0.12 – 0.46 × 10^{-6} m^2/s), C_p (300 – 1800 J/kg K), and density (275 – 1111 kg/m^3). As a comparison between the two groups, the least *k values* are similar, while C_p and α from group II are considerably higher, with about 13 % and 17 %, respectively. However, the highest wall resistivity with 200 mm thickness is observed for HC2, which is about 24 % higher than S2-CA.

3.1.1. Stored energy

As shown in Fig. 13, the stored energy of hemp concrete varies between 2.38 and 5.54 MJ/m^2 after 24 h. However, the values increase significantly with time in the 80 – 110 % range between 6 and 24 h. The highest three values are 5.54, 5.08, and 4.98 MJ/m^2 for alkali-activated mixture walls AAFA-NaOH, AAFA + AAMK, and AAFA-Na_2SiO_3, respectively, which ascribed to their higher $\rho \times C_p$ values. On the other hand, the least three Qs values are observed with lime-binders SF, FA, and MK representing 2.38, 2.57, and 2.84 MJ/m^2, respectively, due to the lower production values of $\rho \times C_p$. Likewise, higher density and heat capacity walls show higher stored energy values. The walls of hempcrete in Fig. 13 might be categorized depending on stored energy into five groups based (on 24 h) to evaluate the performance of individual walls:

- Group I (Stored energy (Qs) = 2.30 – 3.30 MJ/m^2): 14 masonry walls,
- Group II (Stored energy (Qs) = 3.31 – 4.30 MJ/m^2): 9 masonry walls,
- Group III (Stored energy (Qs) = 4.31 – 5.30 MJ/m^2): 2 masonry walls,
- Group IV (Stored energy (Qs) > 5.30 MJ/m^2): 1 masonry wall.

Hempcretes show higher heat capacity values, as depicted in Fig. 10,

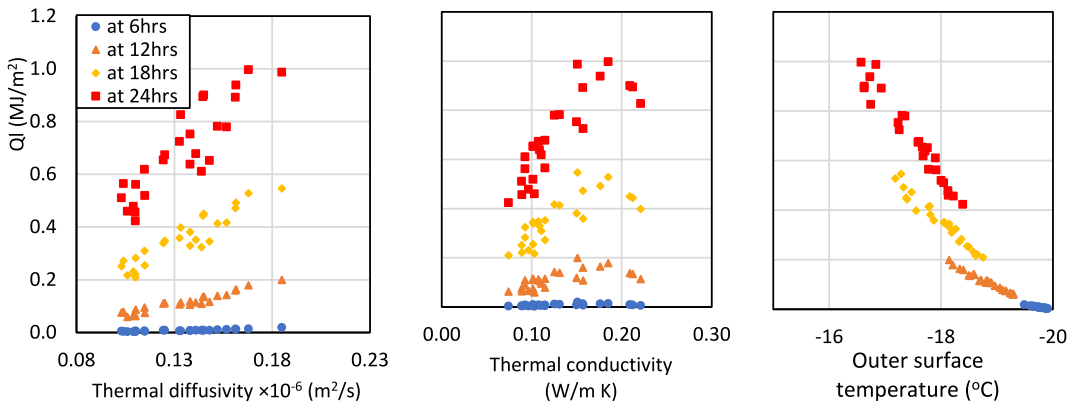

Fig. 15. The relevant between losses of thermal energy and thermal characteristics of hempcrete walls.

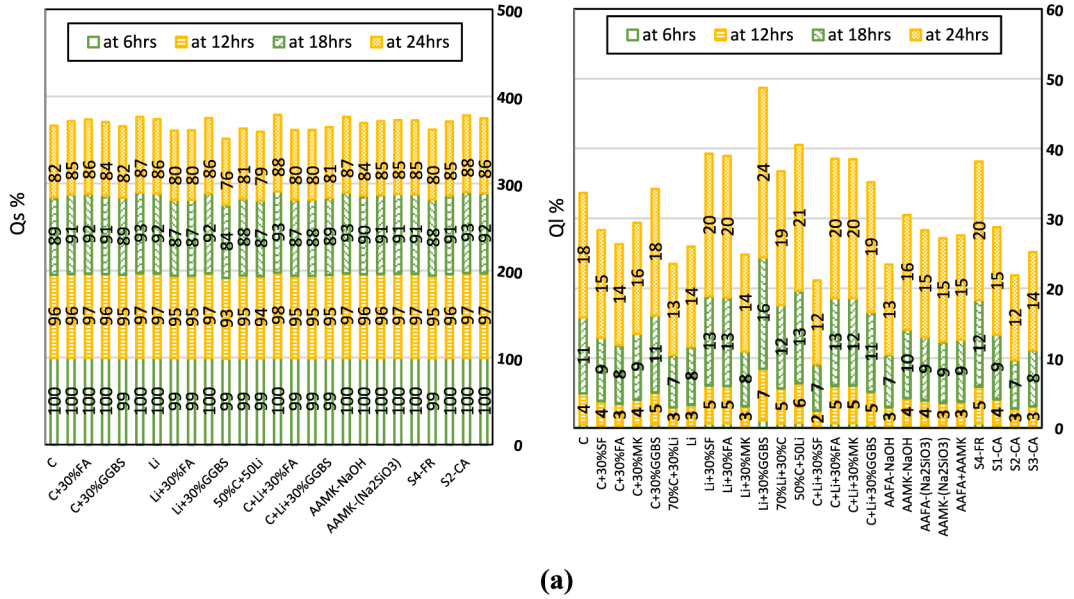

(a)

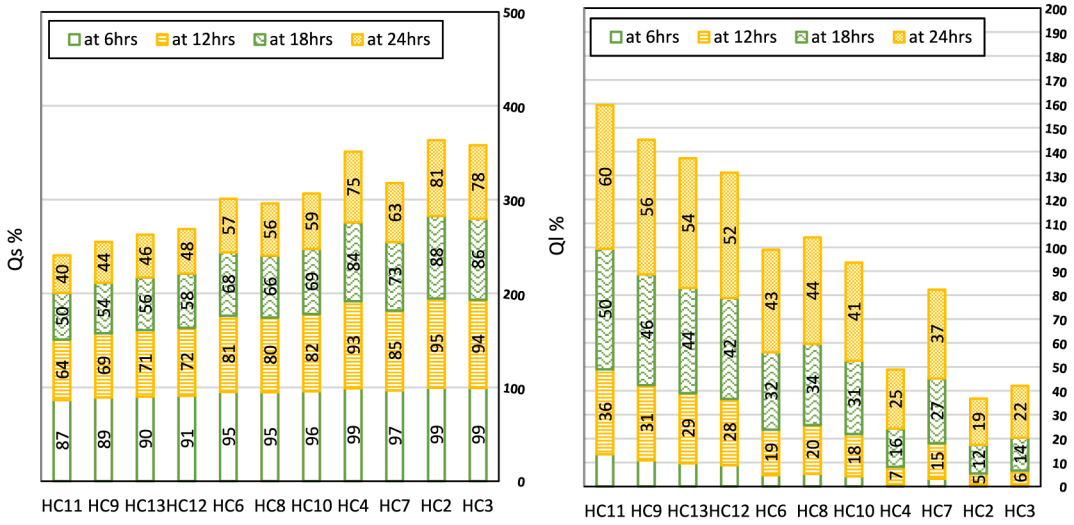

(b)

Fig. 17. Comparison between stored and lost heat energy as percentages for hempcrete from (a) this study and (b) the literature.

while the densities are relatively lower; hence, the Qs values are low, such as Group I walls. On the other hand, Group III and Group IV showed relatively higher values (reaching 56 %) due to the increment of density and heat capacity.

3.1.2. *Lost energy*

The lost energy for hemp concrete showed little value, not exceeding 1.0 MJ/m^2 after 24 h, as shown in Fig. 14. Surprisingly, the lost energy over the first six hours was negligible for all walls. Then, the values increased slightly, revealing a max value of 0.2 MJ/m^2 at 12 h, while loss reached 0.55 MJ/m^2 at 18 h (i.e., about 175 % increment). The lowest value of Ql was observed by the S2-CA mixture with about 0.42 MJ/m2 at 24 h due to the lowest *k values* (about 0.07 W/m K), as shown in Fig. 10. The highest values observed by Li + GGBS and C + Li + MK with 0.99 and 1.0 MJ/m^2, respectively, which attributed to their highest values of conductivity (0.15–0.19 W/m K) and diffusivity (0.18–0.17 × 10^{-6} m^2/s). The walls could be categorized into five groups for their lost energy:

- Group I (Ql = 0.40 – 0.50 MJ/m^2): 4 Walls,
- Group II (Ql = 0.51 – 0.60 MJ/m^2): 4 Walls
- Group III (Ql = 0.61 – 0.70 MJ/m^2): 7 Walls
- Group IV (Ql = 0.71 – 0.80 MJ/m^2): 4 Walls
- Group V (Ql > 0.8 MJ/m^2): 6 Walls

The four walls of Group I showed the least escaped energy due to their lower k-values (0.07, 0.10, 0.10, 0.09 W/m K), while the highest Ql was observed for Group V, which had relatively higher *k-values* (0.18, 0.13, 0.16, 0.19, 0.15, 0.21, 0.21 W/m K).

As shown in Fig. 15, the lost energy increases with increasing the values of thermal conductivity, diffusivity, and outer surface temperature. Thus, the walls with higher thermal properties (k, α) result in higher values of lost energy. Consequently, materials with lower thermal conductivity and diffusivity are desirable for building envelopes and

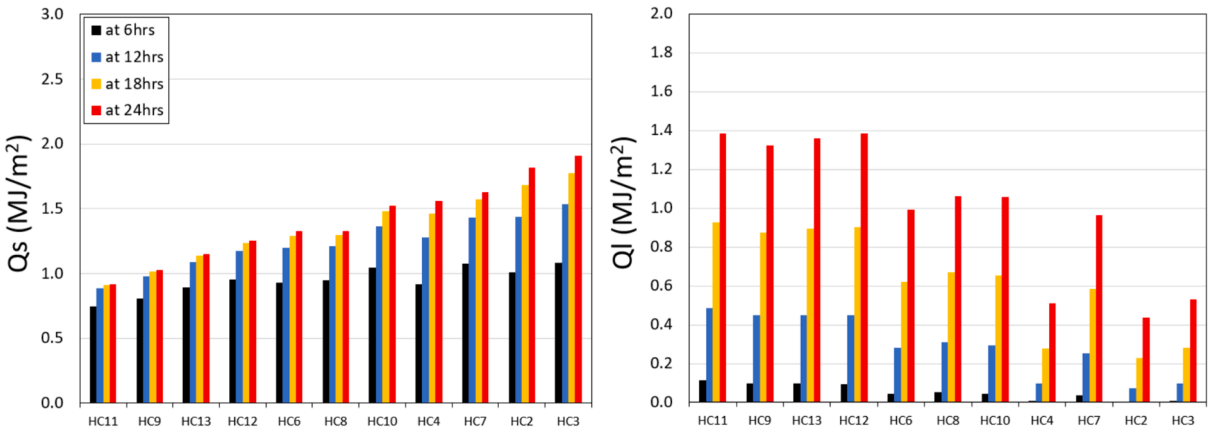

Fig. 16. Stored and lost heat energy values for hempcrete walls, as reported in the literature.

Table 7
Comparison between Qs and Ql values for hempcrete in this study and the literature.

Time (h)	Qs (MJ/m²)		Ql (MJ/m²)	
	This study	Literature	This study	Literature
Over 6	1.33–2.48	0.75–1.08	0.00–0.02	0.01–0.12
Over 12	1.90–4.04	0.88–1.53	0.06–0.20	0.07–0.49
Over 18	2.21–4.95	0.91–1.78	0.21–0.55	0.23–0.93
Over 24	2.38–5.54	0.92–1.91	0.42–1.00	0.44–1.38

Table 8
Comparison between Qs and Ql percentages for hempcrete in this study and the literature.

Time (h)	Qs %		Ql %	
	This study	Literature	This study	Literature
Over 6	100	87–100	0	<13
Over 12	>95	64–94	>5	6–36
Over 18	87–93	50–88	7–13	12–50
Over 24	76–88	40–81	12–24	19–60

thermally efficient performance.

3.1.3. Comparison between stored and lost energy

As a comparison between Qs and Ql, Fig. 17 shows interesting results illustrating no loss at the first 6 h and a minimal loss after 12 h, which proved the superior insulation property of hemp concrete with high storing ability reaching 4 MJ/m^2 at 12 h. At 18 h, the walls start losing considerable heat because of achieving a higher storage capacity, which continues increasing, heading toward the storage capacity limit. A comparison between percentages of stored and lost energy is carried out to assess each wall, which is presented in the next section.

3.2. Comparison between hemp concrete for walls (Literature and experimental data)

Fig. 16 shows the stored and lost energy from the literature hempcrete (Hempcrete I) over 24 h. Obviously, most energy is stored in the first 6 h and slightly continued charging till 24 h, indicating a lower capacity compared to hempcrete II in Fig. 13. Most walls showed a slight energy loss at the first 6 h (3 walls showed almost zero), which hempcrete II similarly observed in Fig. 14.

As summarized in Table 7, the stored energy recorded for hempcrete in this study (Hempcrete II) is significantly higher than that of literature hempcrete walls, reaching 160 – 190 % due to the relatively higher $\rho \times C_p$. Further, the lost energy of these study walls showed a substantially lower value (5 – 40 %) compared to the literature walls due to the lower conductivity, diffusivity, and higher heat capacity.

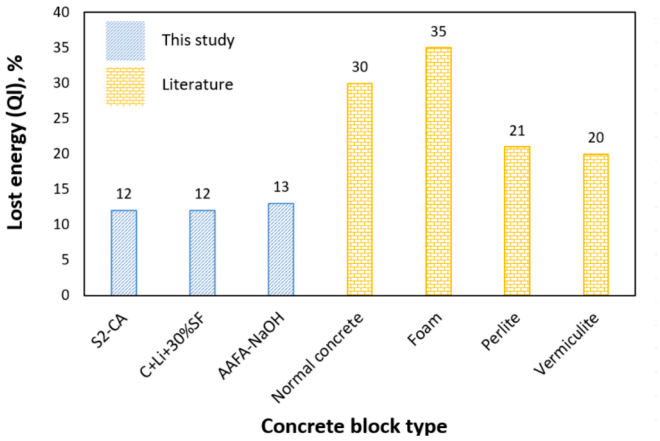

Fig. 18. Comparison between lost energy for concrete blocks from this study and the literature.

For assessing the values of stored and lost thermal energy (Qs and Ql) into/from different hempcrete walls, the percentages of stored energy and corresponding lost energy are calculated and presented in Table 8 and Fig. 17. Hemp concretes produced in this study showed significantly higher stored energy and lower lost thermal energy at each time interval than literature hempcrete (Table 8 and Fig. 17). This may be ascribed to smaller diffusivity values (0.10 – 0.18 $\times$ 10^{-6} m^2/s) for hempcrete produced in this study relative to literature hempcrete (0.12 – 0.46 $\times$ 10^{-6} m^2/s). However, literature hempcrete has a conductivity of (0.06 – 0.12 W/m K) similar to produced hempcrete (0.07 – 0.18 W/m K).

As shown in Table 8 and Fig. 17, the stored energy after 6 h demonstrates about 100 % storing energy (i.e., Ql = 0 %), which proves the high thermal efficiency of hempcrete produced in this study (showing lower diffusivity values in Fig. 10). However, the stored energy reached 76 – 88 % after 24 h (about 12 – 24 % losing energy), which is relatively higher than the literature hempcrete (40 – 81 %), as shown in Fig. 17 (b). From group II data, the minimum percentage of Ql after 24 h is 12 %, representing hempcrete walls S2-CA and C + Li + 30 %SF with the same diffusivity value (0.11 $\times$ 10^{-6} m^2/s). At the same time, the minimum Ql % from literature hempcrete is about 19 % for HC2 with a diffusivity value of 0.12 $\times$ 10^{-6} m^2/s for the same time interval. Interestingly, higher thermal diffusivity hempcrete increased lost energy, as depicted with HC11-9–13 and 12 with diffusivities of 0.46 $\times$ 10^{-6}, 0.40 $\times$ 10^{-6}, 0.38 $\times$ 10^{-6}, 0.37 $\times$ 10^{-6} m^2/s, respectively, showing lost energy of 60,

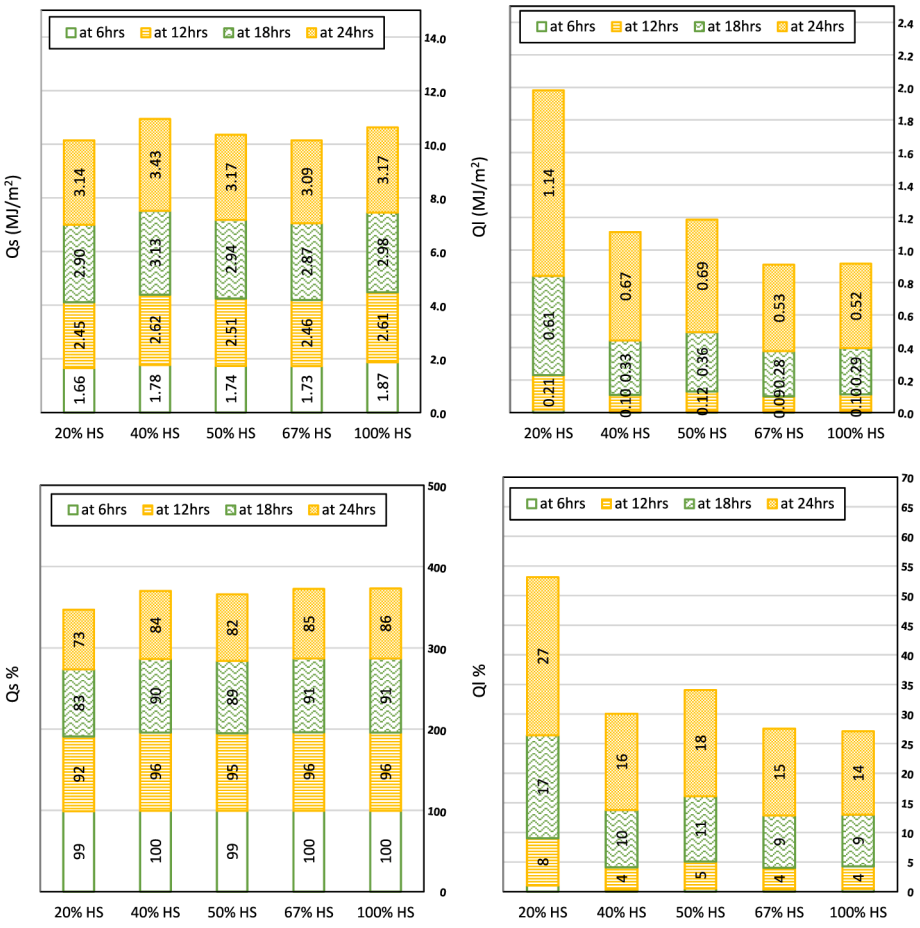

Fig. 19. Stored and lost thermal energy for hempcrete with various hemp contents.

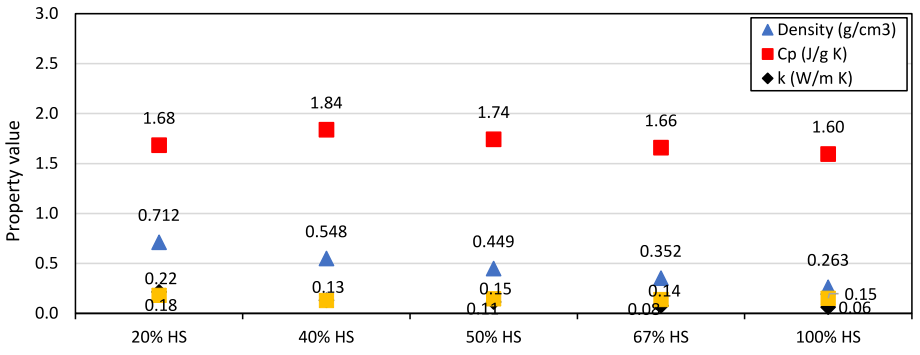

Fig. 20. Thermal properties of hempcrete with different hemp contents.

56, 54, and 52 %, respectively. In conclusion, hempcrete produced in this study showed promising thermal performance for cold weather regions due to the lower lost energy, which is zero lost at 6 h and not exceeding 24 % after 24 h.

Comparing the performance of hempcrete walls to conventional concrete walls, the energy loss in top-tier hempcrete walls is less than 13 %. In contrast, regular concrete, perlite, vermiculite, and foam exhibited energy losses ranging from 21 % to 35 % ([17]), as illustrated in Fig. 18. Thus, hempcrete demonstrates significant potential in manufacturing masonry blocks for constructing building envelopes and conserving heat energy.

3.3. *Effect of hemp content on stored and lost energy*

The experimental data of hempcrete with varying hemp content were used in the model to address the effect of hemp content on stored and lost thermal energy. The results of Qs and Ql are presented as percentages and amounts with their corresponding hemp contents in Fig. 19. The stored energy increases significantly with time from 1.66 – 3.43 MJ/m^2, and the lost energy also increases from 0.01 – 1.14 MJ/m^2 between 6 and 24 h. At 6 h, the stored energy is about 100 %, and minimal lost energy shows superior thermal performance. At 24 h, the stored energy decreased due to increasing lost energy, reaching a maximum percentage of 27 % for a hemp content of 20 %. On the contrary, the least lost energy is observed by 100 % of hemp content, with about 14 %. However, other hemp contents (40 – 67 %) show a 15 – 18 % lost energy.

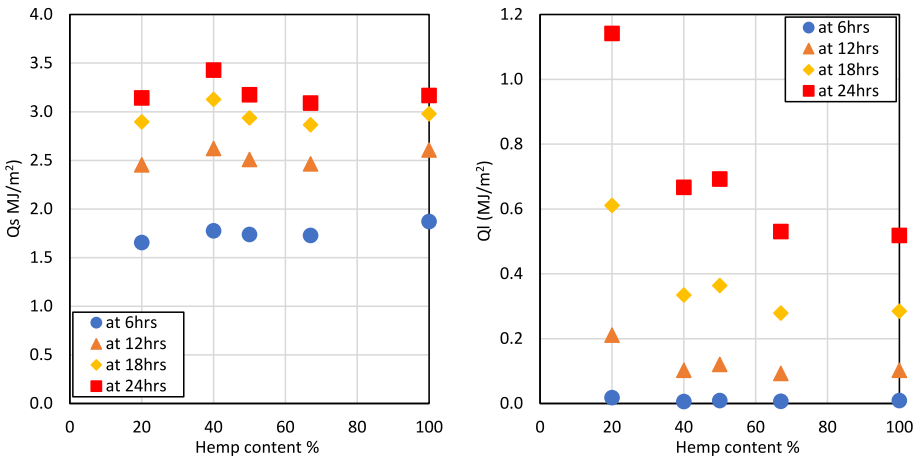

Fig. 21. Correlation between Qs and Ql for hempcrete walls with different hemp content.

Noticeably, the lost energy significantly decreases from 27 % to 16 % with increasing hemp content from 20 % to 40 %, which may be attributed to higher C_p and lower *k values*, as shown in Fig. 20. In summary, the lost energy dropped by 27 – 16 % with increasing hemp content by 20 – 40 %, then the change was relatively lower by 14 – 18 % with higher hemp content by 50 – 100 %.

As shown in Fig. 20, density and C_p values decrease by 40 – 100 % with increasing hemp content, while the stored energy increases slightly from 84 – 86 %. This behavior is ascribed to the appreciable reduction in thermal conductivity of 0.13 – 0.06 W/m K (about 120 %), leading to a slighter decrease in exterior wall temperature. Thus, the lost energy decreased again slightly from 16 – 14 %. Interestingly, 40 % of hemp content showed higher stored energy (i.e., lower Ql) relative to 50 % due to the higher C_p values and the slight reduction in *k values*.

As shown in Fig. 21, the stored energy increased with increasing hemp content over 6 and 12 h. In comparison, the increment is not significant for time over 18 and 24 h due to approaching the maximum capacity of the wall. On the other hand, lost energy decreases with increasing hemp content, showing a higher difference after 12 h, ascribed to the rise in the R-value of walls. Therefore, the presence of more hemp hurds showed higher Qs and lowered Ql due to the enhanced thermal properties. However, the density tends to decrease with higher hemp content due to the light weight of hemp, leading to relatively lower stored energy.

4. Conclusions

This study evaluates the thermal performance of hempcrete masonry walls in terms of energy storage capability and energy loss to the exterior environment, aiming to minimize energy waste and required electric energy for heating purposes in cold zones, as hempcrete showed superior thermal insulation properties (low k and α values), Twenty-five hempcrete were experimentally produced and compared to the reported ones through a simulation (using ANSYS Fluent). The outcomes of this study are summarized as follows:

- The stored energy directly correlates to the product of ρ and C_p value of walls. In comparison, heat loss is remarkably influenced by *k-value* and *α-value*.
- Although hempcrete is lightweight concrete with relatively smaller densities than normal concrete (which decreases its capability of storing higher energy), many hempcrete mixtures produced in this study with alkali-activated binders showed relatively higher density, lower thermal conductivity, and higher heat capacity values. Hence, the newly produced hempcrete's increased stored energy could reach 130 % due to its enhanced density.
- The activated binder group showed the highest stored energy, followed by cement-lime-based binders and lime-based binders, mainly affected by the density and heat capacity of the individual mixture.
- Over 24 h, the maximum stored energy was 1.91 and 5.54 MJ/m^2 for HC3 (literature) and AAFA-NaOH (present study), respectively, with a difference of 190 %. For the minimum energy lost, the values were 0.44 and 0.42 MJ/m^2 for HC2 (literature) and S2-CA (this study), respectively.
- The best performance for storage and energy loss in the literature walls is for HC2 (the lost energy is 0.44 MJ/m^2, and the stored energy is 1.82 MJ/m^2 over 24 h). In comparison, the present hempcrete S2-CA shows lower lost energy of 0.42 MJ/m^2 and higher stored energy of 3.07 MJ/m^2. In addition, a new hempcrete wall C + Li + 30 %SF showed almost the same lost energy of 0.46 MJ/m^2 but with an even higher stored energy of 3.36 MJ/m^2.
- Generally, the hempcrete produced in this study showed a promising thermal performance as the percentage of lost energy for all models is in the range of 12 – 24 %, while that for the literature walls varies between 19 and 60 %. The percentage of stored energy increases with increasing hemp content from 73 to 86 %; hence, the lost energy decreases from 27 to 14 % due to elevated C_p*-value* and depressed *k-value* of hemp. The low density of hemp reduces the Qs values, but using proper binders, e.g., geopolymer binders, increases the density significantly.

CRediT authorship contribution statement

Ahmed S. Al-Tamimi: Writing – original draft, Methodology, Investigation, Formal analysis, Data curation, Conceptualization. **Naef A.A. Qasem:** Writing – review & editing, Writing – original draft, Supervision, Investigation, Formal analysis, Conceptualization. **Vivek Bindiganavile:** Investigation, Data curation, Conceptualization, Supervision, Writing – original draft.

Declaration of competing interest

The authors declare that they have no known competing financial interests or personal relationships that could have appeared to influence the work reported in this paper.

Data availability

No data was used for the research described in the article.

References

[1] S. Real, M.G. Gomes, A. Moret Rodrigues, J.A. Bogas, Contribution of structural lightweight aggregate concrete to the reduction of thermal bridging effect in buildings, Constr. Build Mater. 121 (2016) 460–470, https://doi.org/10.1016/j.conbuildmat.2016.06.018.

[2] Natural Resources Canada. Heating equipment for residential use. NRCAN 2022: 1–4.

[3] Agency USEP. Renewable Heating and Cooling 2016:1–10.

[4] M. Martínez, N. Huygen, J. Sanders, S. Atamturktur, Thermo-fluid dynamic analysis of concrete masonry units via experimental testing and numerical modeling, J. Build. Eng. 19 (2018) 80–90, https://doi.org/10.1016/j.jobe.2018.04.029.

[5] Council Directive 2010/31/EU of the European Parliament. Directive 2010/31/EU of the European Parliament and of the Council of 19 May 2010 on the Energy Performance of Buildings. Optics InfoBase Conference Papers 2010.

[6] Canadian Standards Association. Standards on concrete masonry units-A165 SERIES-14 (R2019). vol. 14. 2014.

[7] National Concrete Masonry Association. ASTM Specifications for Concrete Masonry Units 2012:9.

[8] J.M. Blanco, Y.G. Frómeta, M. Madrid, J. Cuadrado, Thermal performance assessment of walls made of three types of sustainable concrete blocks by means of fem and validated through an extensive measurement campaign, Sustainability (switzerland) 13 (2021) 1–18, https://doi.org/10.3390/su13010386.

[9] W.A. Al-Awsh, N.A.A. Qasem, O.S.B. Al-Amoudi, M.A. Al-Osta, Experimental and numerical investigation on innovative masonry walls for industrial and residential buildings, Appl. Energy 276 (2020) 115496, https://doi.org/10.1016/j.apenergy.2020.115496.

[10] Z. Hongxia, P. Kang, C. Baoquan, L. Xuanyi, Numerical simulation of thermal theory of sintered coal gangue self-insulation block and wall, MATEC Web of Conf. 175 (2018), https://doi.org/10.1051/matecconf/201817501021.

[11] J. Wernery, A. Ben-Ishai, B. Binder, S. Brunner, Aerobrick - an aerogel-filled insulating brick, Energy Procedia 134 (2017) 490–498, https://doi.org/10.1016/j.egypro.2017.09.607.

[12] H. Su, D. Wu, M. Shen, W. Chen, S. Wang, Development and performance test including mechanical and thermal of new tenon composite block masonry walls, Adv. Mater. Sci. Eng. (2019), https://doi.org/10.1155/2019/5253946.

[13] K. Kant, A. Shukla, A. Sharma, Heat transfer studies of building brick containing phase change materials, Sol. Energy 155 (2017) 1233–1242, https://doi.org/10.1016/j.solener.2017.07.072.

[14] A.S. Al-Tamimi, O.S. Baghabra Al-Amoudi, M.A. Al-Osta, M.R. Ali, A. Ahmad, Effect of insulation materials and cavity layout on heat transfer of concrete masonry hollow blocks, Constr. Build. Mater. 254 (2020) 119300, https://doi.org/10.1016/j.conbuildmat.2020.119300.

[15] Baghabra O, Al-Osta M, Al-Tamimi A. THERMAL INSULATING MASONRY HOLLOW BRICKS. US 10,538,916 B1, 2020.

[16] R. Haik, A. Peled, I.A. Meir, Thermal performance of alternative binders lime hemp concrete (LHC) building: comparison with conventional building materials, Build. Res. Inf. 49 (2021) 763–776, https://doi.org/10.1080/09613218.2021.1889950.

[17] N.A.A. Qasem, A.S. Al-Tamimi, V. Bindiganavile, Thermal energy storage and losses in various types of masonry concrete walls, J Energy Storage 67 (2023) 107555, https://doi.org/10.1016/j.est.2023.107555.

[18] Bergman T, Lavine A, Incropera F, Dewitt D. Fundamentals of Heat and Mass Transfer. 7th ed. n.d.

[19] A. Reilly, O. Kinnane, F.J. Lesage, G. McGranaghan, S. Pavía, R. Walker, et al., The thermal diffusivity of hemp-lime, and a method of direct measurement, Constr. Build Mater. 212 (2019) 707–715, https://doi.org/10.1016/j.conbuildmat.2019.03.264.

[20] E. Gourlay, P. Glé, S. Marceau, C. Foy, S. Moscardelli, Effect of water content on the acoustical and thermal properties of hemp concretes, Constr. Build Mater. 139 (2017) 513–523, https://doi.org/10.1016/j.conbuildmat.2016.11.018.

[21] P. De Bruijn, P. Johansson, Moisture fixation and thermal properties of lime-hemp concrete, Constr. Build Mater. 47 (2013) 1235–1242, https://doi.org/10.1016/j.conbuildmat.2013.06.006.

[22] A.D. Tran Le, C. Maalouf, T.H. Mai, E. Wurtz, F. Collet, Transient hygrothermal behavior of a hemp concrete building envelope, Energ. Build. 42 (2010) 1797–1806, https://doi.org/10.1016/j.enbuild.2010.05.016.

[23] Ahlberg J, Georges E, Norlén M. The potential of hemp buildings in different climates 2014.

[24] V.D. Gorgots, Standard Practice for Selecting Proportions for Normal, Heavyweight, and Mass Concrete (ACI 211.1-91), Donald. (2002).

[25] A. Peschard, A. Govin, P. Grosseau, B. Guilhot, R. Guyonnet, Effect of polysaccharides on the hydration of cement paste at early ages, Cem. Concr. Res. 34 (2004) 2153–2158, https://doi.org/10.1016/j.cemconres.2004.04.001.

[26] S. Pantawee, T. Sinsiri, C. Jaturapitakkul, P. Chindaprasirt, Utilization of hemp concrete using hemp shiv as coarse aggregate with aluminium sulfate [Al2(SO4)3] and hydrated lime [Ca(OH)2] treatment, Constr. Build Mater. 156 (2017) 435–442, https://doi.org/10.1016/j.conbuildmat.2017.08.181.

[27] Eroglu S., Toprak S., Urgan O, MD, Ozge E. Onur, MD, Arzu Denizbasi, MD, Haldun Akoglu, MD, Cigdem Ozpolat, MD, Ebru Akoglu M. Hemp Industrial Production and Uses. vol. 33. 2012.

[28] T. Jami, S.R. Karade, L.P. Singh, A review of the properties of hemp concrete for green building applications, J. Clean. Prod. 239 (2019) 117852, https://doi.org/10.1016/j.jclepro.2019.117852.

[29] Walker R. A Study of the Properties of Lime-Hemp Concrete with Pozzolans. 2013.

[30] A. Evrard, A. De Herde, Bioclimatic envelopes made of lime and hemp concrete, Proceeding of CISBAT 2005 (2005) 1–6.

[31] Z. Li, L. Wang, X. Wang, Compressive and flexural properties of hemp fiber reinforced concrete, Fibers Polym. 5 (2004) 187–197, https://doi.org/10.1007/BF02902998.

[32] ISO 22007. Determination of thermal conductivity and thermal diffusivity. International Standard ISO 22007-1:2017(E) 2017;2017.

[33] M. Mamun, F. Batool, V. Bindiganavile, Thermo-mechanical properties of fibre reinforced cement-based foam exposed to sulphate, Constr. Build Mater. 61 (2014) 312–319, https://doi.org/10.1016/j.conbuildmat.2014.03.006.